NACA TN 4072 9040

TECH LIBRARY KAFB, NM
0066943

NATIONAL ADVISORY COMMITTEE FOR AERONAUTICS

TECHNICAL NOTE 4072

EXPERIMENTAL INVESTIGATION OF ATTENUATION OF STRONG SHOCK WAVES IN A SHOCK TUBE WITH HYDROGEN AND HELIUM AS DRIVER GASES

By Jim J. Jones

Langley Aeronautical Laboratory
Langley Field, Va.

Washington
July 1957

AFMDC
TECHNICAL LIBRARY
AFL 2811

1L

TECH LIBRARY KAFB, NM
0066943

NATIONAL ADVISORY COMMITTEE FOR AERONAUTI

TECHNICAL NOTE 4072

EXPERIMENTAL INVESTIGATION OF ATTENUATION OF STRONG SHOCK WAVES IN A SHOCK TUBE WITH HYDROGEN AND HELIUM AS DRIVER GASES

By Jim J. Jones

SUMMARY

An experimental investigation has been made of the attenuation of strong shock waves in air in a shock tube. Time-history measurements were made of the static pressure at several stations in the wall of the tube. The internal diameter of the tube is 3.75 inches. Shock-wave-velocity data were taken for a distance along the tube of about 120 feet. The range of the shock-wave Mach number covered was from 5 to $10\frac{1}{2}$ and the initial pressure ahead of the shock wave varied from 5 to 100 millimeters of mercury. Hydrogen and helium were used as driver gases.

A helium-driven shock wave was found to decay only about one-half as rapidly as a hydrogen-driven shock wave. The pressure level had little effect on the attenuation rate of a shock wave of given strength for the pressure range investigated. The static-pressure measurements indicated that a severe pressure gradient existed in the latter portion of the air flow. This gradient limits the testing time useful for obtaining reliable aerodynamic data.

INTRODUCTION

The shock tube has become a practical facility for obtaining aerodynamic data in simulation of hypersonic flight. High stagnation-temperature flows are rather easily produced in the shock tube, and high flow Mach numbers may be obtained by expanding the flow through a nozzle. (See, for example, ref. 1.)

The inherent shortcoming of the shock tube is, of course, the very short testing time. Some increase in testing time is possible by increasing the linear dimensions of the tube. However, the tube must of necessity be long if strong shock waves are considered because the

testing time, the time interval between the arrival of the shock wave and the contact surface (the term "contact surface" is used throughout to designate what is in reality a mixing zone between the air and the driver gas), at any station decreases with increasing shock-wave Mach number. The increase in testing time obtained by increasing the tube length is limited because the attenuation of the shock wave is considerable in traveling through a tube which is many diameters long. Thus, as the tube becomes longer, the difficulty of obtaining the desired strength of shock wave at the test section increases. Furthermore, the growth of the boundary layer in the tube causes a variation with time of the flow properties behind the wave. This variation may be large and thus may limit the usefulness of the facility in obtaining aerodynamic data. The diameter of the tube must be as large as practical to alleviate this problem.

Much work has been done to determine, both experimentally and analytically, the attenuation of weak shock waves in shock tubes. (See, for example, refs. 2 to 6.) However, above a shock-wave Mach number of about 5, very little experimental work has been published and the analytic work is limited to the realm of perfect gases. The need for such data above a Mach number of 5 becomes increasingly important because greater and greater emphasis is being placed on the shock tube as a hypersonic test apparatus. The purpose of the present paper is to present the results of an experimental investigation to measure the attenuation of strong shock waves in a 3.75-inch-diameter shock tube in which helium and hydrogen were used as driver gases.

SYMBOLS

l	distance traveled by flow
M_s	shock-wave Mach number
p_1	initial pressure in low-pressure chamber, lb/sq in.
p_4	initial pressure in high-pressure chamber, lb/sq in.
R	Reynolds number
T_1	initial temperature in low-pressure chamber, $^{\circ}R$
T_o	stagnation temperature behind shock wave, $^{\circ}R$
T_w	wall temperature, $^{\circ}R$

t	time, milliseconds
u	computed velocity immediately behind shock wave
u_s	shock-wave velocity
x	axial distance from diaphragm station, ft
γ	ratio of specific heats
ν	kinematic viscosity based on free-stream conditions
ρ_1	density ahead of shock wave, slugs/cu ft
ρ_r	reference density, 0.002509 slugs/cu ft

APPARATUS

Shock Tube

A layout of the shock tube and some of the related equipment is shown in figure 1. The tube has a constant internal diameter of 3.75 inches. The high-pressure chamber is 14 feet 2 inches long and was made by boring out a 90-millimeter antiaircraft gun barrel. The working pressure of the gun barrel is in excess of 25,000 pounds per square inch. The first 47 feet of the low-pressure chamber downstream from the diaphragm was made of heavy-wall carbon-steel tubing which had a wall thickness of 0.375 inch. The working pressure of this tubing was 3,300 pounds per square inch. The inside surface of this tubing was nickel plated to resist corrosion. The rest of the low-pressure tubing was stainless steel, with a wall thickness of 0.125 inch and a working pressure of 1,000 pounds per square inch. Approximately 260 feet of this stainless-steel tubing was available; however, data were not obtained for this total length as the shock tube was usually operated at shorter lengths. Since none of the tubing used for the low-pressure chamber was machined on the inside surface, some axially alined scratches or grooves caused by the extruding process remained. The quality of the joints between lengths of tubing is not known accurately, as inspection after assembly was difficult. However, in designing and machining the joints and tubing, an attempt was made to eliminate any crack and hold the misalinement to ±0.002 inch.

The high-pressure chamber rode on skids and could be moved a short distance in the direction of its axis to facilitate installing and

removing diaphragms. This movement was accomplished by a large hydraulic ram. The force developed by the ram was used to hold and seal the diaphragm.

The low-pressure chamber was evacuated to the desired pressure through a port near the downstream end. The gases were admitted to the high-pressure chamber through the extreme upstream end opposite the diaphragm station. The bottled supply of these gases was stored a short distance away. The valves that controlled the gases were located near the high-pressure chamber and were operated by long torque tubes from the instrument and control building.

A casemate enclosed the high-pressure chamber on three sides. The casemate was made of concrete walls backed by banked earth. In the photograph of figure 1 the shock tube is shown exposed; however, in normal operation it was shielded from sun and rain by an aluminum cover.

Diaphragms

The main diaphragm used to separate the two chambers was made of steel, aluminum, or copper. A cross-shaped mark was first scribed to a given depth on one face to provide parting lines at rupture. This prescribing prevented pieces of the diaphragm from shearing off and being carried downstream. Also, varying the depth of the scribe marks to some extent allowed a systematic variation of diaphragm rupture strength. Inasmuch as the diaphragms were ruptured by pressure rather than any mechanical device, the scribe depth was controlled as carefully as possible to control rupture strength.

A second diaphragm was used at the extreme downstream end of the low-pressure chamber. This diaphragm was made of photographic film and was ruptured by the arrival of the shock wave.

Shock-Wave Detection

The principal means of detecting the passage of the shock wave was ionization gaps. For this purpose, automobile 10-millimeter spark plugs mounted in the wall of the tube were used on the early runs. Later, plugs were machined which did not have the ground electrode and in which the insulator, which was Teflon, came flush with the wall. A stronger signal was obtained if the center electrode protruded about 1/64 inch into the stream. The gap between the center electrode and the case (ground) was about 0.050 inch for the machined plugs.

The circuits used in connection with the ionization gaps are shown in figure 2. If the output of a station was displayed on an oscilloscope,

the circuit of figure 2(a) was used. The output of the circuit shown in figure 2(b), which employed a thyratron tube, was connected to an electronic counter. Either circuit depends upon a reduction in the resistance across the gap to produce a signal.

The locations of the stations at which plugs were mounted in the tube are given in figure 1. Not every plug was used for each run.

Pressure Measurements

Pressure measurements were obtained along the wall of the tube at several stations. Two different types of pressure transducers were used in obtaining the data presented. One was a variable-capacitance-type gage manufactured by the Rutishauser Corporation and the other was a SLM quartz piezoelectric crystal. Most of the pressure data were obtained with the SLM pressure pickup. The pressure attained in the high-pressure chamber just prior to diaphragm burst was measured with a strain-gage type of pressure cell connected to the high-pressure chamber with a short nipple and was recorded in the instrument building. Maximum error of this measurement is estimated to be within ±20 pounds per square inch. The pressure in the low-pressure chamber was read just prior to diaphragm burst on an absolute pressure gage. One such gage was mounted in the instrument building. Because of the slow response due to the long tubing connection to this gage, another gage was mounted close to the shock tube with a short connection. The readings of these two gages were compared and the measurement p_1 is believed to be accurate within ±0.2 millimeters of mercury.

RESULTS AND DISCUSSION

Shock-Wave Velocity Measurements

Typical oscilloscope records showing signals obtained from the pressure pickup and from the ionization gaps are presented as figure 3. The records were obtained on a drum camera at a film speed of 1 inch per millisecond. The signals from three different ionization-gap stations on the same run are shown. A sharp rise in signal which quickly decays indicates the shock wave as it passes a station. A second rise in signal follows which drops with the apparent arrival of the contact surface. The decay of the first signal and the onset of the second signal are unexplained. The assumption that the end of the second signal coincides with the arrival of the contact surface is borne out by comparision with the theoretical position of the contact surface. The

fact that the arrival of the shock wave coincided with the first signal was verified by mounting a pressure pickup beside an ionization gap. No difference in the time of arrival of the shock wave could be discerned between the two methods as long as the shock wave was strong enough to produce a signal from the ionization gap. No disturbance in the pressure record consistently coincided with the arrival of the second signal from the ionization gap. The first signal (fig. 3(b)) is not as strong for stations farther down the tube where the shock wave has decayed in strength. However, the second signal was stronger for the stations farther down the tube under certain test conditions, as shown, for example, in the sample record. The pressure record shown in figure 3(a) was not obtained on the same run as the ionization-gap record of figure 3(b).

The circuit used with the electronic counters employed a thyratron tube which required a certain signal strength to fire. If the shock wave were weak, the first signal might be insufficient to fire the thyratron, which might then fire on the rise of the second signal. The firing on the rise of the second signal would give an erroneous reading on the counter. Therefore, the counters were generally used with the stations close to the diaphragm where the shock wave was strongest while the oscilloscopes were used with the stations farther downstream. However, for comparison purposes and in order to detect an erroneous reading on the counter, oscilloscope records were also obtained for some stations close to the diaphragm.

The data obtained from the counters and the oscilloscope records were plotted as shown in figure 4 and the curves faired through the data points. The local velocity of the shock wave was then taken as the slope of the faired curve. The slope of the faired curve was assumed to be equal to the slope of straight-line segments connecting points on the curve that represent a distance 4 feet apart. These velocities were then plotted in the form of shock-wave Mach number M_s against the distance of the shock wave from the diaphragm station x as shown in figures 5 to 8.

Figure 5 shows typical shock-wave attenuation when a hydrogen driver is used. The data are shown for various shock-wave strengths at given values of the pressure ahead of the shock wave p_1 where the pressure range of p_1 is from 5 to 100 millimeters of mercury. The shock-wave Mach number usually increases for a short distance, reaches a maximum, and then decreases in a nearly linear manner. The fact that the shock wave reaches its maximum strength as far as 20 feet downstream from its origin may be attributed to the finite time required for the diaphragm to open fully. (A single measurement indicated a time of the order of 400 microseconds from the time of rupture until the diaphragm is open fully.) This shock-wave formation distance appears to be slightly larger for the higher values of shock-wave Mach number.

The termination of the data in most cases represents the farthest distance downstream that the shock-wave passage could be detected and measured accurately with the detection and data-reduction system used.

For the purpose of comparison, the theoretical shock-wave Mach numbers corresponding to the initial conditions of each run are shown in the keys of figures 5 to 7. The real gas effects in the air were considered in computing the theoretical shock-wave Mach number.

Figure 6 shows typical shock-wave attenuation when helium is used as a driver gas. The principal difference in effects of the two drivers (other than pressure ratio required to attain a given shock-wave Mach number) is the rate at which the shock waves decay. When helium is the driver, the slope of the curves after the maximum values of M_s is reached is only about one-half as great as for a hydrogen-driven shock. This difference in attenuation due to driver gas is very apparent in figure 7, which compares a hydrogen-driven shock wave with two helium-driven shock waves, one having about the same maximum shock-wave Mach number and the other having about the same initial pressure p_1.

The difference in shock-wave attenuation for the two driver gases tested is evidently due to a difference in the waves being generated in the driver gas itself. In reference 5, an analysis based on the assumption of perfect gases (and therefore limited to relatively weak shock waves) was developed and indicated that the sign of the waves generated as a result of skin friction in the driver gas changes at a critical flow Mach number which is equal to $\frac{1}{\gamma - 1}$. When the flow Mach number in the driver gas is greater than the critical value, the effect of skin friction is to generate downstream compression waves; when the flow Mach number is smaller than the critical value, the effect of skin friction is to generate expansion waves. The results of the present tests seem to indicate a similar effect for strong shock waves, at least in a general way. That is, for the hydrogen-driven shock wave of figure 7 where the flow Mach number in the hydrogen was about 2.5, the total attenuating effects were much greater than for the helium-driven shock wave having the same peak strength, where the flow Mach number in the helium was about 7.9. Thus, while hydrogen is the more efficient driver in the sense that a smaller diaphragm pressure ratio $\frac{p_4}{p_1}$ is required to produce a given shock-wave strength, the attenuating effects for hydrogen are greater than for helium.

In reference 6 (applicable for thin boundary layers and relatively weak shock waves), the critical flow Mach number mentioned previously in this report does not appear and the driver gas contributed only compression waves. However, the strength of these waves is found to be affected by the effects of heat transfer in the driver gas; thus, the difference in attenuation might be due to the difference in heat transfer

in the hydrogen and helium. Another influencing factor is the reflection effects of the waves at the contact surface.

Certain shock-wave data from figure 5 have been replotted in figure 8 to determine if there is any noticeable effect of initial pressure on attenuation. Two groups of curves are shown in figure 8, one having a common diaphragm pressure ratio of about 4,500 and the other having a ratio of about 1,000. Hydrogen was used as the driver gas for the data shown. Within the pressure range shown in figure 8, no appreciable dependence of the attenuation rate on pressure level can be discerned. Some change was expected because of the change in Reynolds number; however, the Reynolds number dependence may be so small that it is not evident in the limited range of pressure presented in this report. These experiments indicate, at least, that the effect of pressure level on attenuation is less than indicated in the analyses of references 5 and 6. In each of these analyses, which make the assumption of small total attenuation, an attenuation parameter is developed which is inversely proportional to $p_1^{1/5}$ for the case of a turbulent boundary layer having a 1/7-power velocity profile.

In figure 9 the maximum shock-wave Mach number measured is shown for a number of runs for both helium and hydrogen drivers. Also shown are the calculated curves for both the case of constant fluid properties in the two gases and the case of real gas properties for air but constant fluid properties in the driver gases. The values used in the calculation for real gas properties for air were taken from reference 7 and the initial conditions were taken as $T_1 = 491^\circ$ R and $\rho_1/\rho_r = 0.008$. The shift of these curves with changing initial density is inappreciable for the density range covered experimentally. The experimental shock-wave strengths occur in the range expected except for the strongest shock waves produced with the helium driver. The shock wave for these runs has a higher peak Mach number than that predicted by either calculation for the given diaphragm pressure ratio. This effect cannot be accounted for by taking into account the real gas properties of helium.

Pressure Measurements

In consideration of the very sizable shock-wave attenuation, the region of flow behind the shock wave is not expected to have constant pressure. A pressure gradient with time was measured in other investigations (see, for instance, refs. 5 and 8) and, in fact, a gradient was predicted by the linear theory of reference 5.

In figure 10(a), the typical pressure obtained with the pressure pickup is repeated from figure 3(a). It may be seen that the pressure history may be represented approximately by two straight lines. Immediately after the arrival of the shock wave, there is an interval for which

the pressure gradient with time is very small. For most of the conditions tested, this first gradient is zero within the accuracy of the records and therefore is referred to as the period of constant pressure. Immediately after this period of constant pressure, an approximately linear gradient of increasing pressure appears and continues until the arrival of the contact surface. In the record of figure 10(a), the contact surface arrives at about 1.8 milliseconds. As explained previously, the arrival of the contact surface is taken to coincide with the decay of the second signal from the ionization-gap station.

The sudden change in pressure gradient possibly is the result of boundary-layer transition on the wall. Inasmuch as the turbulent boundary layer grows in thickness more rapidly than a laminar boundary layer, the effective area of the tube would decrease more quickly and thus result in a strong positive pressure gradient with time. No transition experiments have as yet been made in this shock tube for comparison purposes.

If the shock tube is to be used as a facility for obtaining aerodynamic data, it is important that the pressure gradient with time at the test section not be large. For instance, any data obtained during the latter part of the run shown in figure 10(a), where the pressure doubled its original value in a little over a millisecond, would be of extremely doubtful value. A different and more severe limit on usable running time of the shock tube is thus imposed: the data must be obtained during the period when the pressure change is small.

A number of measurements were made to gain a little more information about the time at which the sharp pressure gradient begins. The pressure pickup was mounted at six different axial stations in the wall of the shock tube. With the pickup at each station, the tube was operated at four selected conditions. The results of this survey are summarized in figure 10. The period of constant pressure, defined as the time before the arrival of the sharp pressure gradient (even though some slight change in pressure may be detected before the pressure gradient), is shown for the various axial positions tested. Also shown is the traversal of the contact surface as determined approximately from the ionization-gap signals. This survey indicates that the period of constant pressure, which varies somewhat with distance from the diaphragm, does not persist over approximately 0.5 millisecond for the data shown, and, when compared with the total duration of air flow, represents a severe limitation on testing time.

Reynolds numbers of the flow at the start of the pressure gradient have been computed for the runs presented in figure 10. The Reynolds number is taken here as $R = \frac{ul}{\nu}$ where u is the computed velocity immediately behind the shock wave as it passes over the station of the

pressure pickup, ν is the corresponding kinematic viscosity arbitrarily based on free-stream conditions (real gas effects considered), and l is the distance traveled by the flow which arrives at the pressure pickup at the same instant as the strong pressure gradient. Eliminating l and expressing the Reynolds number in terms of the time t, as presented in figure 10, lead to

$$R = \frac{u^2 t}{\nu\left(1 - \frac{u}{u_s}\right)} \tag{1}$$

where u_s is the shock-wave velocity.

The Reynolds numbers computed from equation (1) for the runs presented in figure 10 are given in the following table:

Figure	x = 23.3 ft	x = 45.8 ft	x = 68.2 ft	x = 90.5 ft
	Reynolds number			
10(b)	30.8×10^6	26.3×10^6	26.7×10^6	20.0×10^6
10(c)	28.8	29.0	26.0	21.8
10(d)	20.2	19.3	18.6	10.9
10(e)	22.6	22.4	22.2	12.7
	T_w/T_o			
10(b)	0.094	0.109	0.119	0.142
10(c)	.088	.094	.104	.127
10(d)	.088	.094	.104	.127
10(e)	.076	.081	.089	.104

Also presented in the table are the corresponding values of the ratio of wall temperature to perfect-gas stagnation temperature of the flow. These values illustrate the very high rate of boundary-layer cooling. This cooling would be expected to stabilize the boundary layer and delay transition. For a given run, the Reynolds number decreases and the value of T_w/T_o increases as the value of x increases. Thus, as expected, greater boundary-layer cooling delays transition. However, even for the limited range of the four runs presented, it is not possible to relate transition Reynolds number to boundary-layer cooling rate alone.

Even if the assumption is made that it is the arrival of boundary-layer transition which is detected by the pressure pickup, it would not

seem justifiable to interpret these transition Reynolds numbers in terms of steady-flow Reynolds numbers, because no equivalence has been established. Indeed, the significance of Reynolds number as defined by equation (1) is open to question.

CONCLUSIONS

An experimental investigation has been made in a shock tube to study shock-wave attenuation for shock Mach numbers in the range 5 to $10\frac{1}{2}$. Hydrogen or helium was used in the high-pressure chamber and air in the low-pressure chamber. The data were obtained in a tube having an internal diameter of 3.75 inches for a distance from the diaphragm up to 120 feet. The most significant findings of the investigation were:

1. For the pressure range of 5 to 100 millimeters of mercury, the pressure in the low-pressure chamber did not significantly affect the attenuation of a shock wave of given initial strength.

2. A helium-driven shock wave decayed only about one-half as rapidly as a hydrogen-driven shock wave.

3. With a hydrogen driver, the maximum Mach number that the shock wave attained for a given diaphragm pressure ratio is in good agreement with theory in which real properties for air are considered. With a helium driver, however, the maximum shock Mach number exceeded the prediction of theory, particularly for large diaphragm pressure ratios.

4. Measurements of the static pressure in the air behind the shock wave show an interval for which the pressure is nearly constant. After this interval a gradient of increasing pressure with time occurs. The time interval of constant pressure was dependent on the distance from the diaphragm and on the strength of shock wave within the range tested. The constant-pressure interval was always less than the time of arrival of the contact surface at the measuring station except possibly for very small distances from the diaphragm station. Thus, a different and more severe limit is placed on usable running time because, in most cases, the pressure gradient is too great to permit reliable aerodynamic data.

Langley Aeronautical Laboratory,
National Advisory Committee for Aeronautics,
Langley Field, Va., May 21, 1957.

REFERENCES

1. Hertzberg, A., Smith, W. E., Glick, H. S., and Squire, W.: Modifications of the Shock Tube for the Generation of Hypersonic Flow. AEDC-TN-55-15 (AD-789-A-2) (Contract No. AF 40(600)-6), Arnold Eng. Dev. Center, Mar. 1955.

2. Donaldson, Coleman duP., and Sullivan, Roger D.: The Effect of Wall Friction on the Strength of Shock Waves in Tubes and Hydraulic Jumps in Channels. NACA TN 1942, 1949.

3. Emrich, R. J., and Curtis, C. W.: Attenuation in the Shock Tube. Jour. Appl. Phys., vol. 24, no. 3, Mar. 1953, pp. 360-363.

4. Hollyer, Robert N., Jr.: A Study of Attenuation in the Shock Tube. Project M720-4 (Contract No. N6-ONR-232-TO IV), Eng. Res. Inst., Univ. of Michigan, July 1953.

5. Trimpi, Robert L., and Cohen, Nathaniel B.: A Theory for Predicting the Flow of Real Gases in Shock Tubes With Experimental Verification. NACA TN 3375, 1955.

6. Mirels, Harold: Attenuation in a Shock Tube Due to Unsteady-Boundary-Layer Action. NACA TN 3278, 1956.

7. Hirschfelder, Joseph O., and Curtiss, Charles F.: Thermodynamic Properties of Air, II. CM-518 (Contract NOrd 9938, Task WIS-1-A), Univ. of Wisconsin, Naval Res. Lab., Dec. 21, 1948.

8. Emrich, Raymond J., and Peterson, Robert L.: Pressure Variation With Time in the Shock Tube. Tech. Rep. No. 7, Project NR 061-063 (Contract N7onr39302), Lehigh Univ., Inst. Res., Mar. 15, 1956.

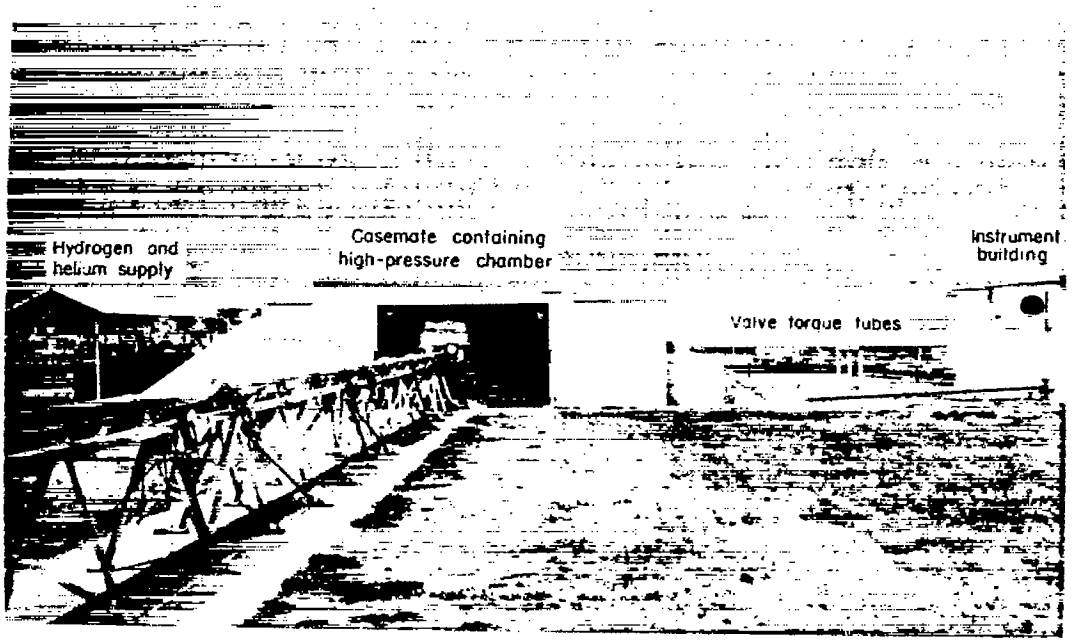

L-94083.1

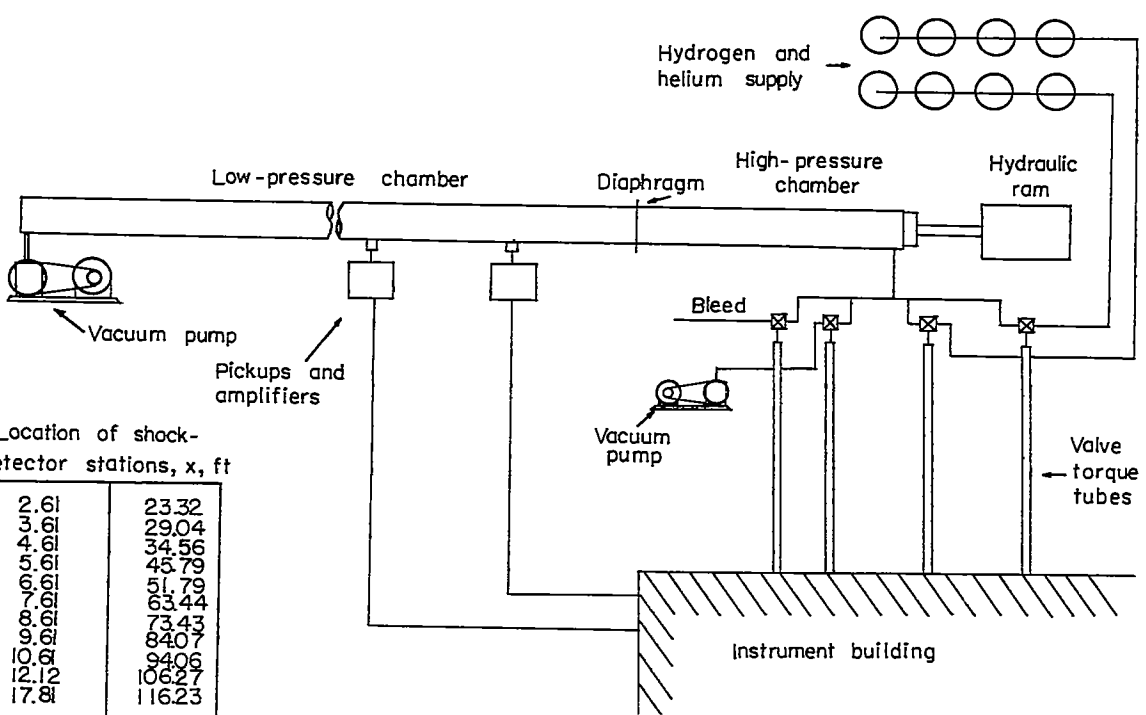

Location of shock-detector stations, x, ft

2.61	23.32
3.61	29.04
4.61	34.56
5.61	45.79
6.61	51.79
7.61	63.44
8.61	73.43
9.61	84.07
10.61	94.06
12.12	106.27
17.81	116.23

Figure 1.- Shock-tube layout.

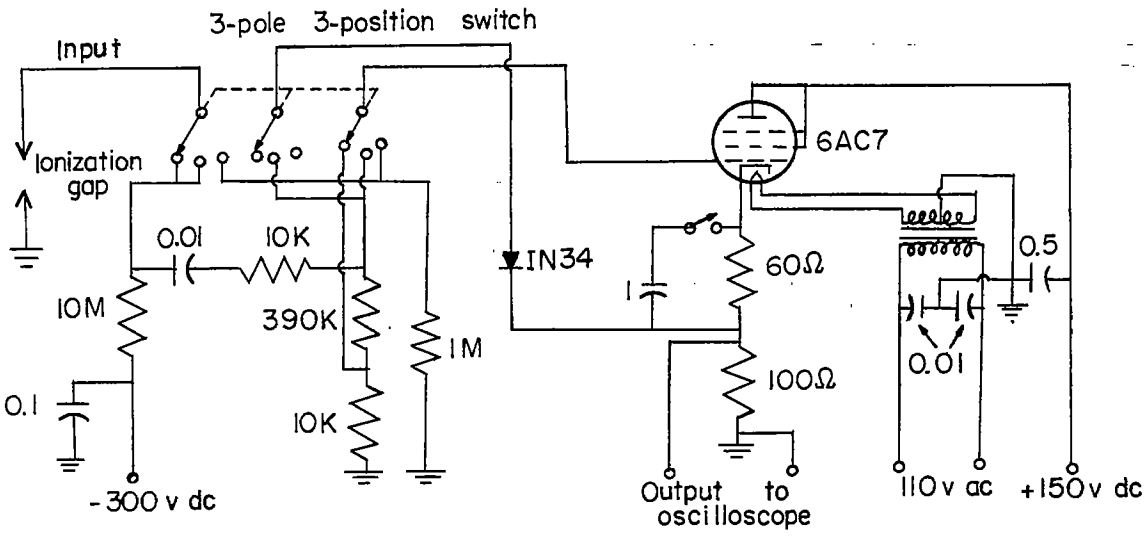

(a) Oscilloscope.

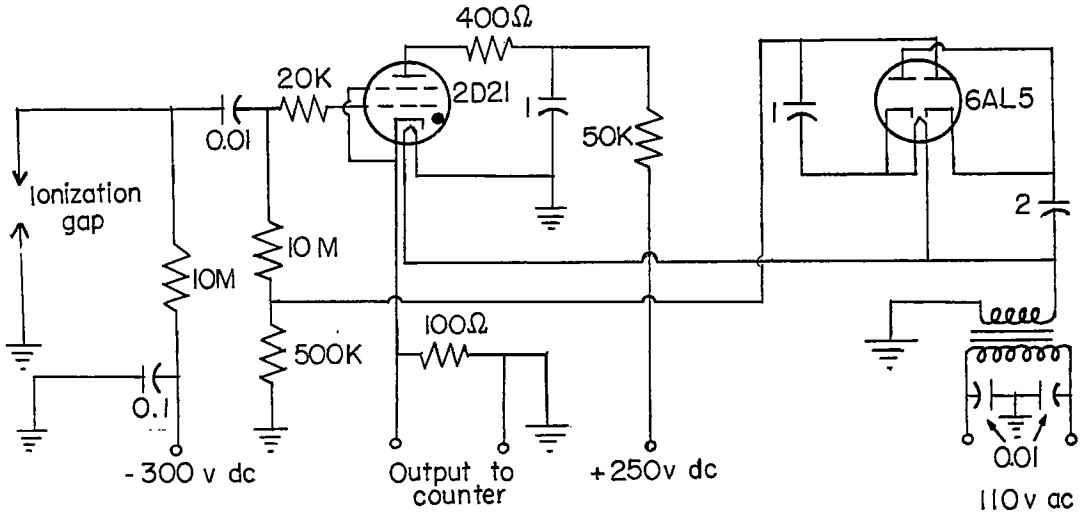

(b) Electronic counter circuit.

Figure 2.- Circuit diagrams for use with oscilloscope and counter. (Values of all capacitors given in microfarads. K = 1,000 ohms; M = 1,000,000 ohms.)

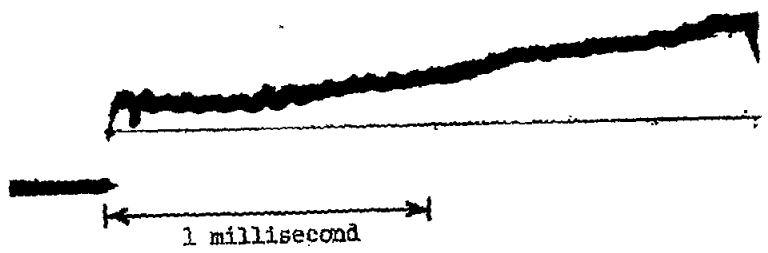

(a) Pressure-pickup record.

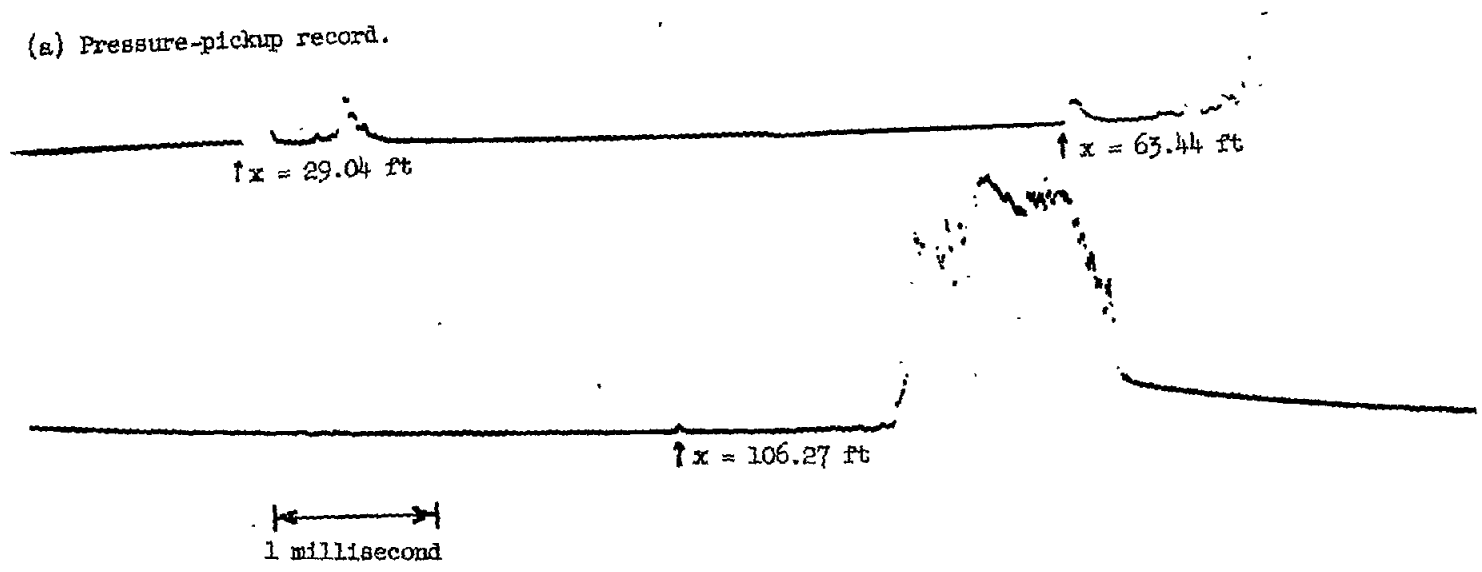

(b) Ionization-gap signals. (Arrow indicates arrival of the shock wave.)

Figure 3.- Typical oscilloscope records of pressure pickup and ionization-gap signals.

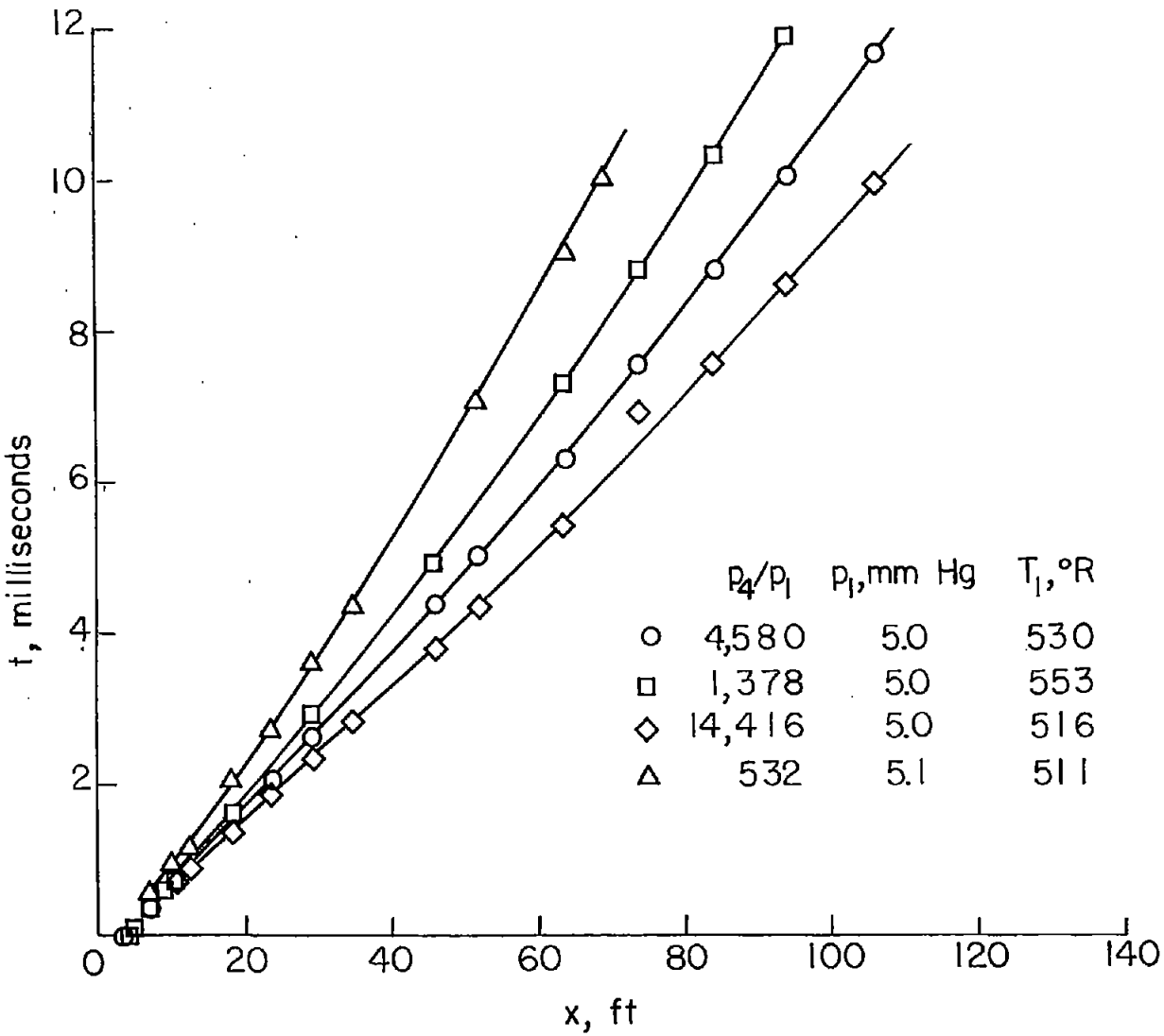

Figure 4.- Typical time-history data of the shock wave.

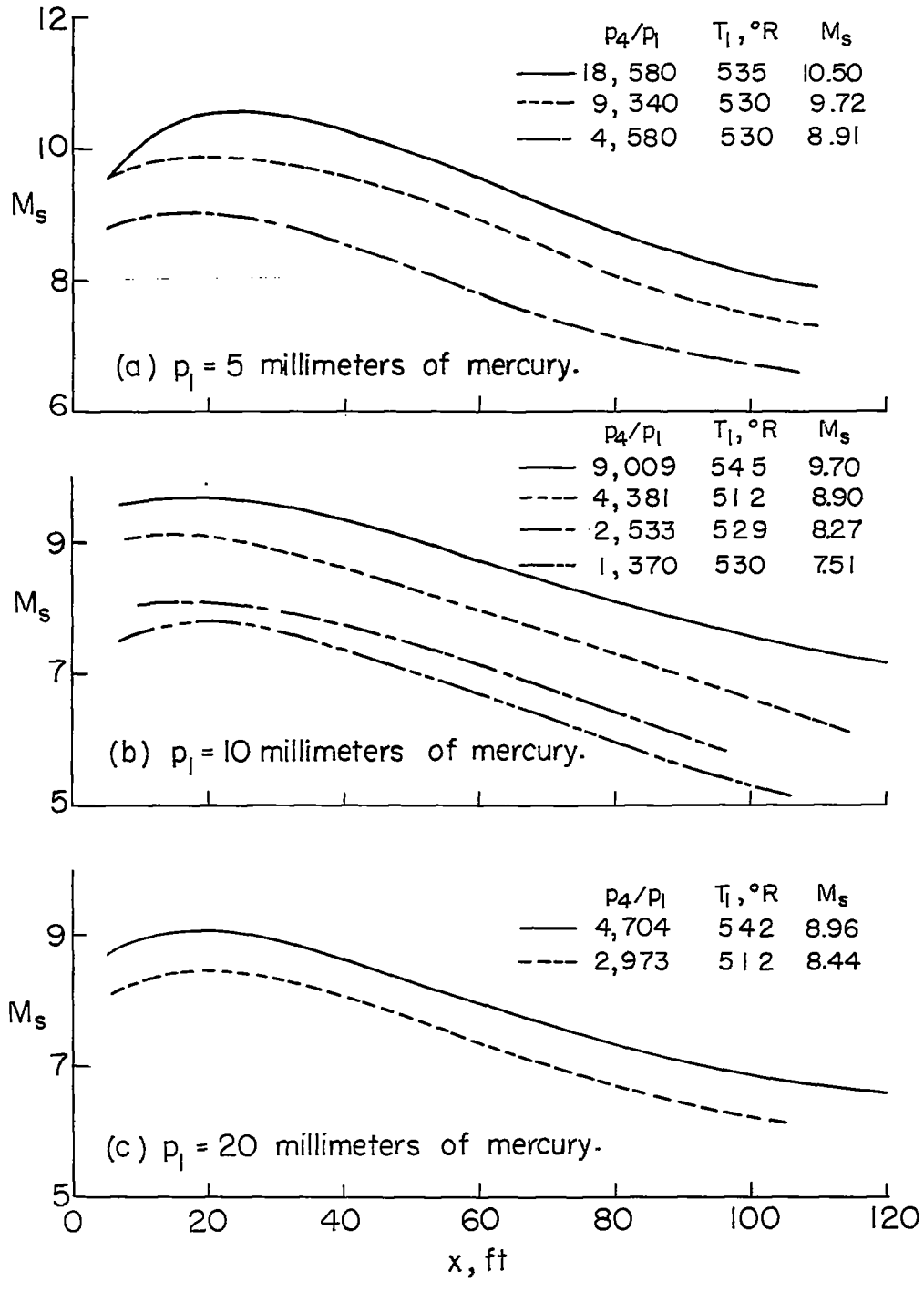

Figure 5.- Typical shock-wave attenuation data with hydrogen as driver gas.

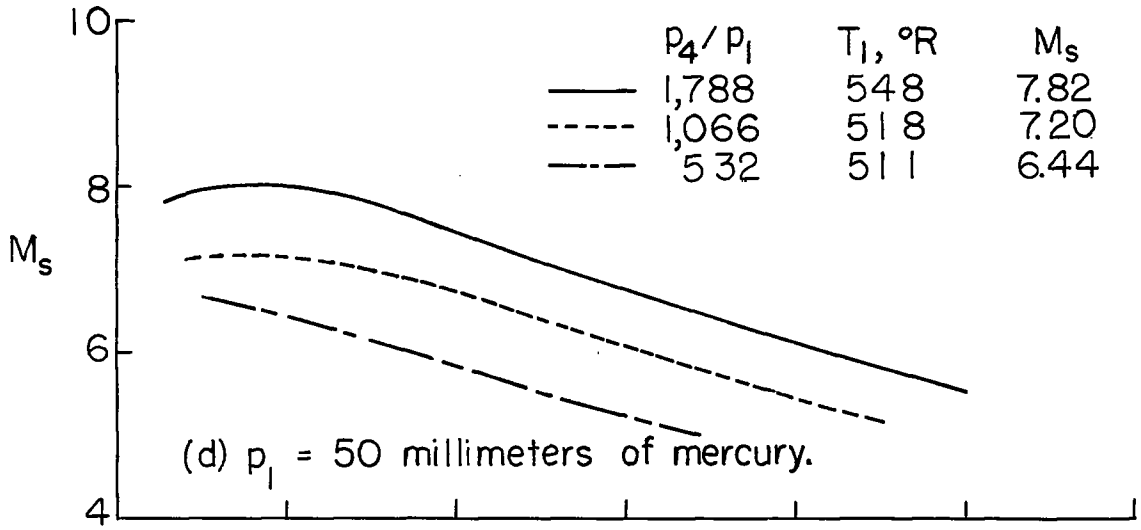

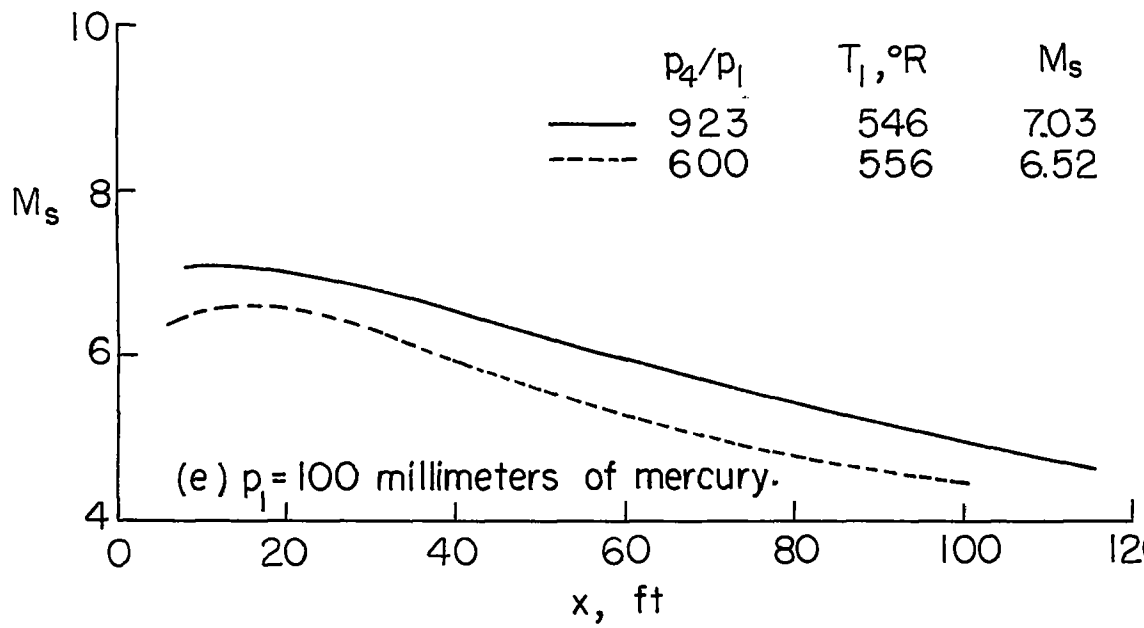

Figure 5.- Concluded.

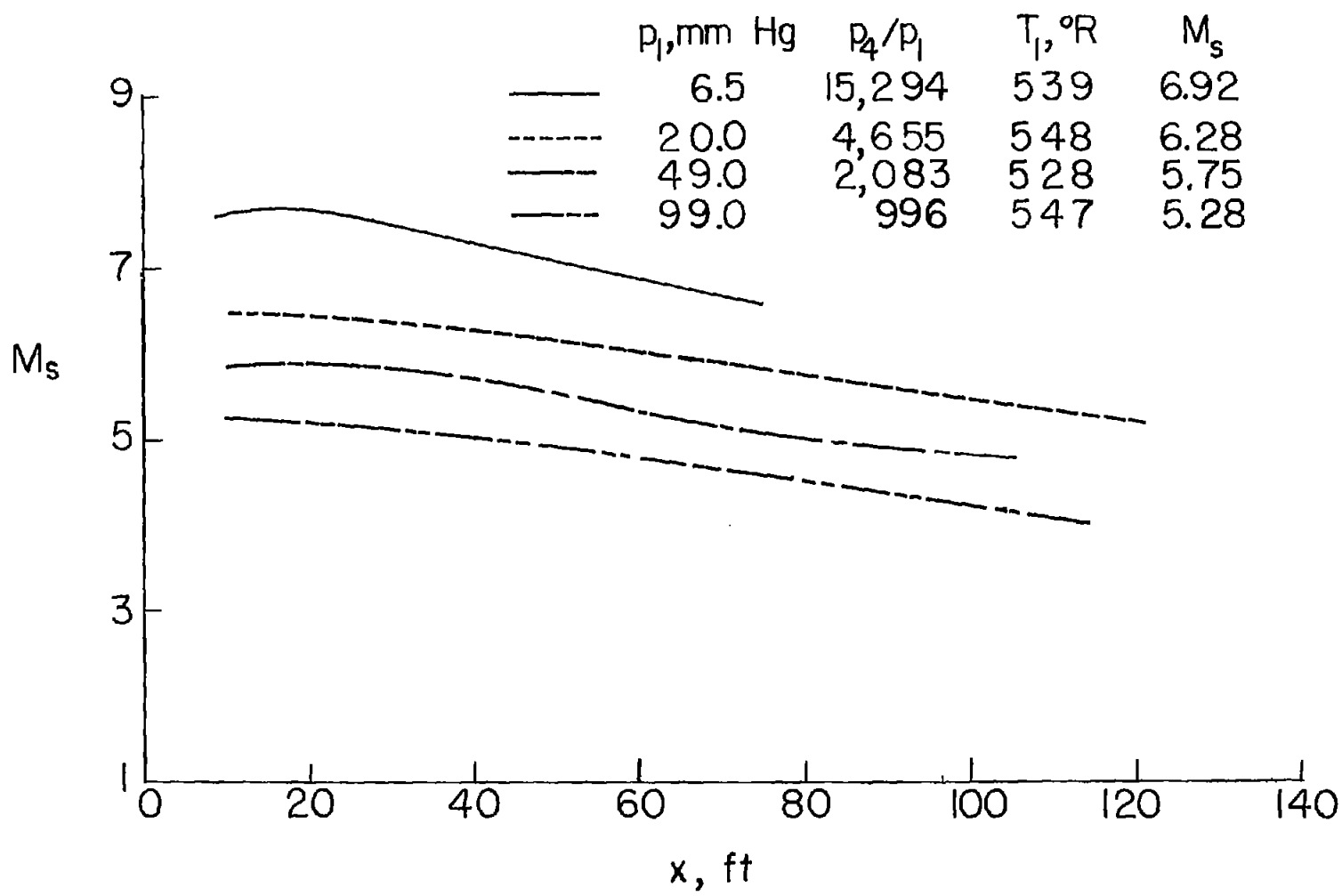

Figure 6.- Typical shock-wave attenuation data with helium as driver gas.

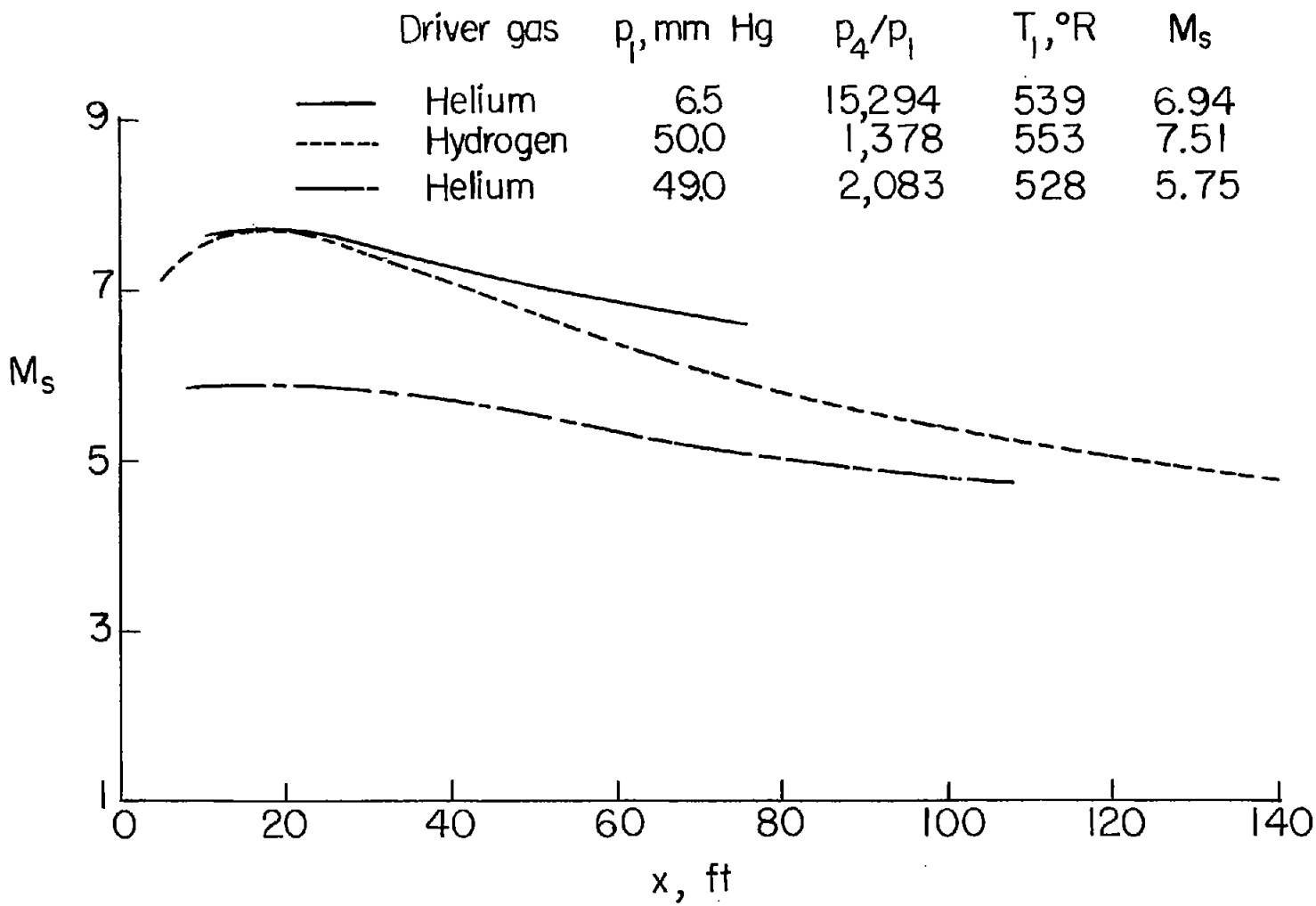

Figure 7.- Comparison of the effects of hydrogen and helium driver gases on shock-wave attenuation.

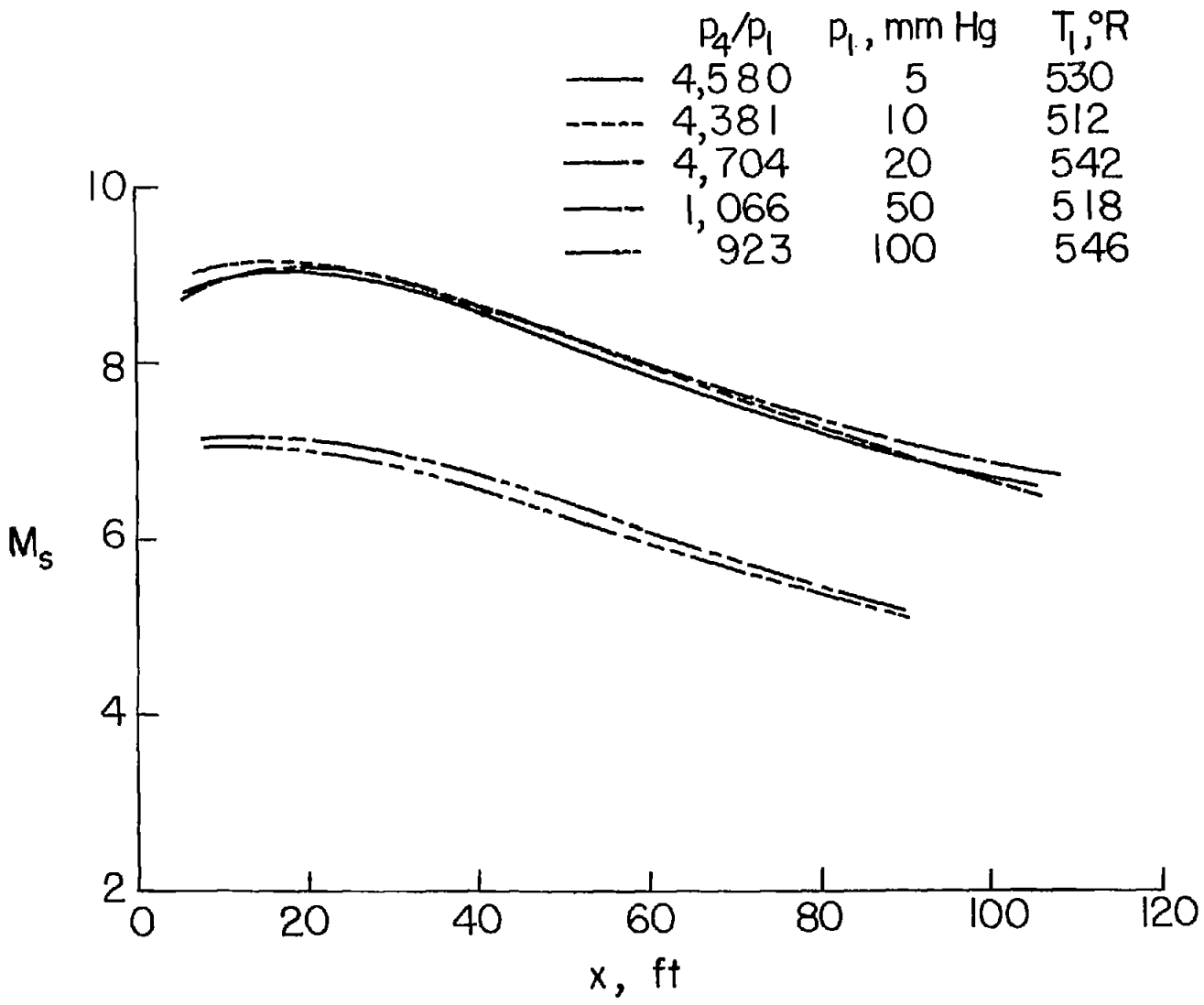

Figure 8.- Effect of initial pressure on attenuation with hydrogen as driver gas.

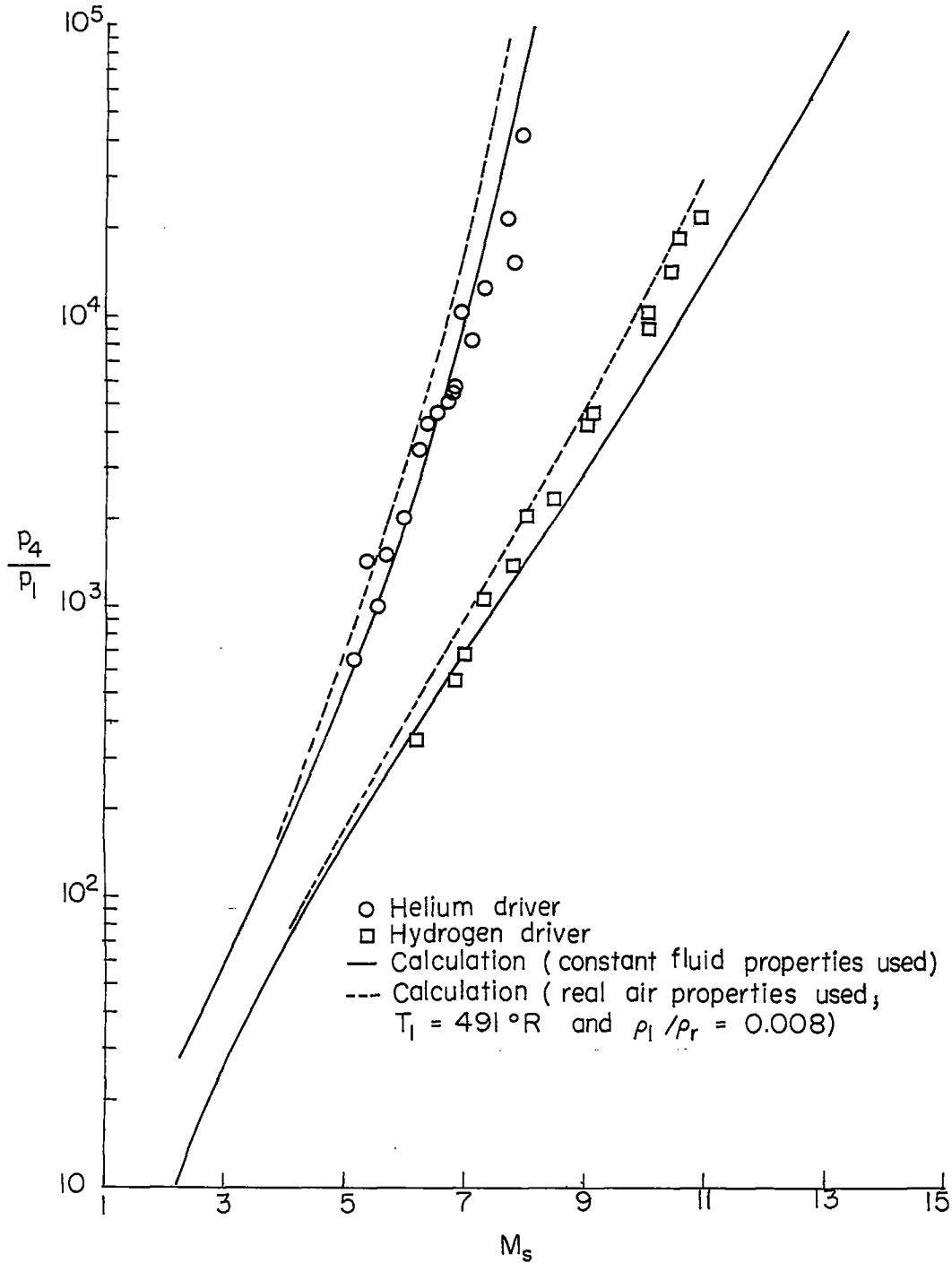

Figure 9.- Comparison of theoretical and experimental shock-wave strengths.

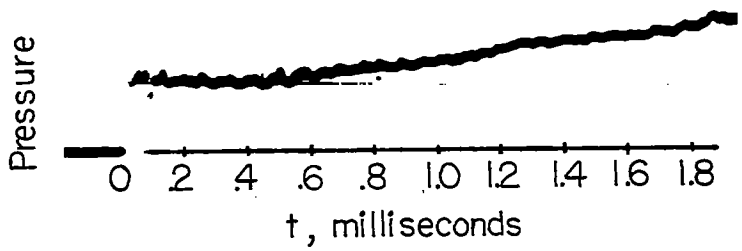

(a) Typical pressure-indicator record.

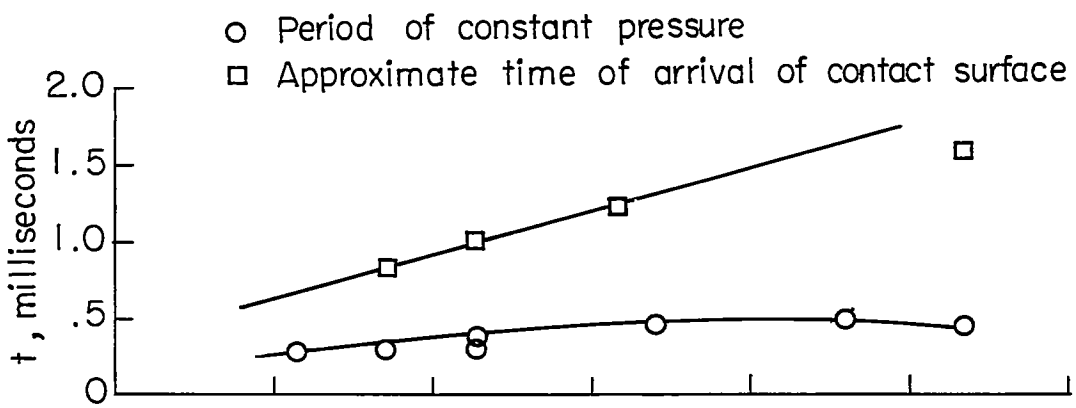

(b) p_1 = 20 millimeters of mercury; $p_4/p_1 \approx 1{,}250$.

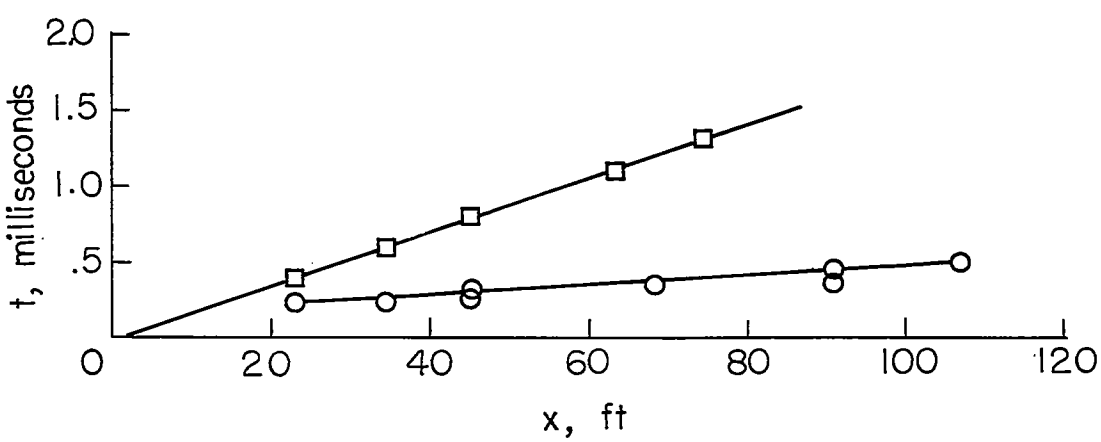

(c) p_1 = 20 millimeters of mercury; $p_4/p_1 \approx 2{,}500$.

Figure 10.- Results of pressure survey along shock tube with hydrogen as driver gas.

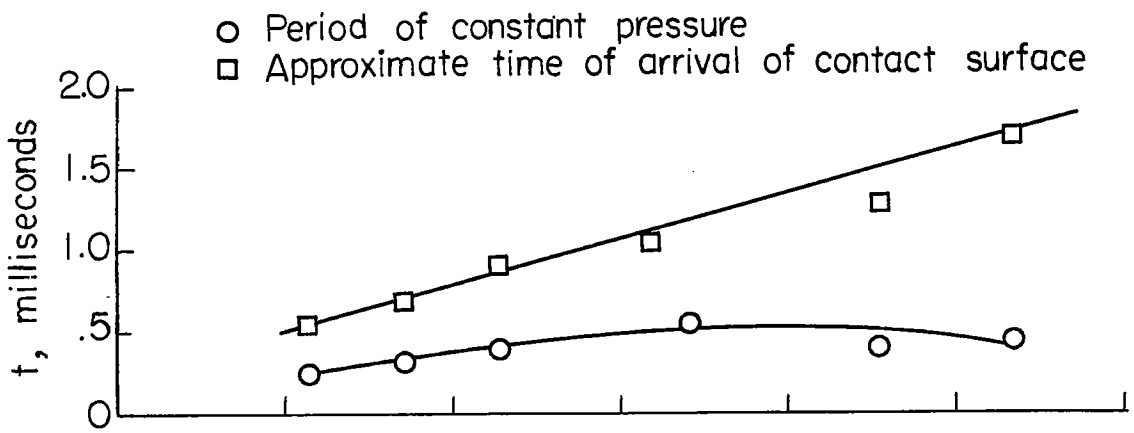

(d) p_1 = 10 millimeters of mercury; $p_4/p_1 \approx 2{,}500$.

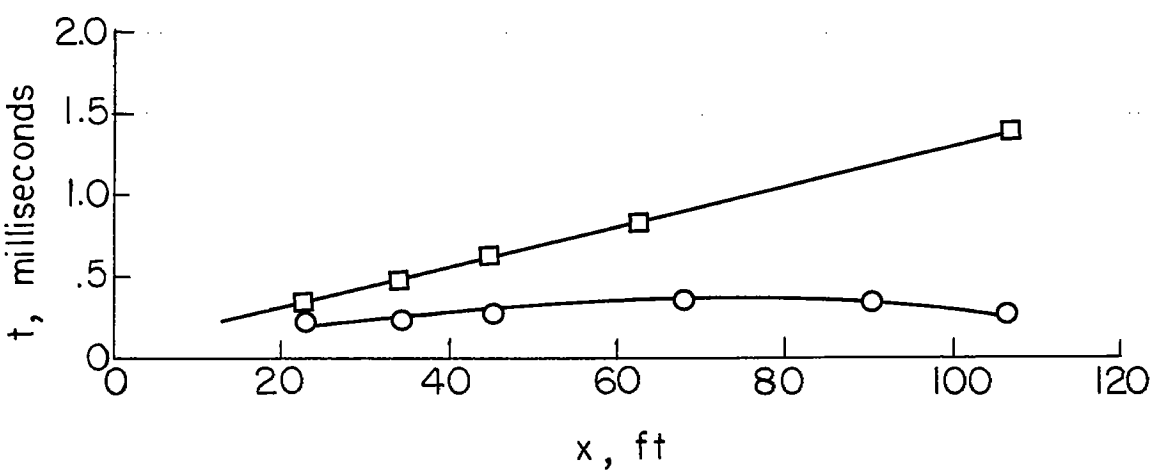

(e) p_1 = 10 millimeters of mercury; $p_4/p_1 \approx 5{,}000$.

Figure 10.- Concluded.